JOURNAL OF GEOPHYSICAL RESEARCH, VOL. ???, XXXX, DOI:10.1029/,

Constraining Atmosphere Models by Assimilation of Atmospheric Angular Momentum

Lisa Neef[1] and Katja Matthes[1]

Corresponding author: L.J. Neef, Düsternbrooker Weg 20, D-24105 Kiel, Germany (neef@geomar.de)

[1]Ocean Circulation and Climate Dynamics - Marine Meteorology, Helmholtz Centre for Ocean Research Kiel (GEOMAR), Kiel, Germany.

Abstract. (Type abstract here)

1. Introduction

1. Common Ground

(i) Atmospheric angular momentum is a global measure of a model's wind and mass distributions.

(ii) AAM can be used to evaluate atmospheric models and reanalyses relative to each other. Even though they are constrained by a large amount of observations, reanalysis sets can still differ significantly in their AAM [*Lehmann and Nevir*, 2012].

(iii) What really makes AAM a useful quantity for evaluating a model or dataset is the fact that it is can be observed, in the form of variations in Earth rotation. On timescales ranging roughly from a few weeks to a few years, changes in the Earth's rotation rate are driven primarily by exchange of axial angular momentum between the solid Earth and the atmosphere. Similarly, wobbles in the orientation of Earth's rotational pole (so-called polar motion) are largely driven by changes in the equatorial components of AAM, though here angular momentum from the oceans and continental hydrosphere also play a significant role, [CITE.]). Thus AAM is observed via three Earth rotation parameters (hereafter ERPs): two angles of polar motion, and anomalies in the length-of-day.

(iv) In order to simulate real events using a climate model, the model state must be somehow brought close to observations. This is frequently done by "nudging" the state to some observed quantities

2. State-of-the-art

• *Saynisch et al.* [2011a, b] and *Saynisch and Thomas* [2012] performed somewhat similar experiments, using four-dimensional DA methods to fit the excitation of ERPs

in an ocean model to the observed oceanic component of ERP excitation, by adjusting boundary parameters (atmospheric wind stresses and freshwater flux). Those studies found that strong adjustments must be made in boundary parameters in order to close the observed discrepancy in the oceanic angular momentum budget. However, these studies did not show whether the assimilation of ERPs actually brought the modeled ocean state closer to reality, i.e. whether the implied adjustments were physically acceptable.

3. **Problems**

• However, while a simple comparison between modeled AAM and observed Earth rotation variations can be helpful [Here it would be awesome to cite an example of where this was done!], it is in general not obvous where or how a model state should be corrected in order to improve the fit between modeled AAM and observed ERPs.

• ...Problems with nudging?...

4. **Solution**

• This study investigates the potential for observed ERPs parameters to constrain the dynamics of an atmosphere model, by constraining its total angular momentum, via ensemble data assimilation.

• Perfect-model experiments show that assimilating the atmospheric component of Earth rotation improves the modeled wind (and pressure?) fields

• Comparison to a common nudging algorithm shows the benefit of assimilating a global integral

• A case study shows the modeled NAO is brought closer to the true state.

5. **Costs / benefits**:

- Why is this better than some sort of nudging?

2. Methodology

2.1. Atmospheric Model and Data Assimilation

Assimilation experiments are performed using the Community Atmosphere Model 5 [*Neale et al.*, 2011, CAM5 hereafter], within the Data Assimilation Research Testbed (DART, *Anderson et al.* [2009], *Raeder et al.* [2012]). CAM5 is run with the finite-volume dynamical core at 2.5 deg. horizontal resolution and 30 hybrid-coordinate vertical levels, with a top near 3 hPa. How is CAM damped at the top? CAM5 forms the atmospheric component of the Community Earth System Model (CESM).

DART is an open-source, community facility that makes ensemble data assimilation available for any model, using any observations. It is available online at `www.image.ucar.edu/DAReS/DART`.

In ensemble data assimilation, covariances between components of the model state and the observations are estimated using an ensemble, which itself is updated with the observed information at each analysis time. Though the DART distribution includes several types of ensemble filter, its primary setting, and the one used in this study, is the deterministic ensemble adjustment Kalman filter [*Anderson*, 2001, EAKF] with a sequential parallel implementation [*Anderson and Collins*, 2007].

2.2. Synthetic Observations

2.2.1. Atmospheric Angular Momentum Observations

The relationship between ERP variations and AAM is given by nondimensional atmospheric excitation functions (AEFs), i.e. nondimensional functions of the three compo-

nents of AAM. These are derived in *Barnes et al.* [1983], and are given by the following:

$$\chi_1(t) = \frac{1.608}{\Omega\,(C-A')}\left[0.684\Omega\Delta\mathbf{I}_{13}(t)+\Delta h_1(t)\right] \quad (1)$$

$$\chi_2(t) = \frac{1.608}{\Omega\,(C-A')}\left[0.684\Omega\Delta\mathbf{I}_{23}(t)+\Delta h_2(t)\right] \quad (2)$$

$$\chi_3(t) = \frac{0.997}{\Omega C_m}\left[0.750\Omega\Delta\mathbf{I}_{33}(t)+\Delta h_3(t)\right] \quad (3)$$

where the $\mathbf{I}_{ij}$ represent components of the atmospheric inertia tensor:

$$I_{13} = -\int R^2\cos\phi\sin\phi\cos\lambda dM \quad (4)$$

$$I_{23} = -\int R^2\cos\phi\sin\phi\sin\lambda dM \quad (5)$$

$$I_{33} = \int R^2\cos^2\phi dM \quad (6)$$

$$(7)$$

and the h_i represent the relative angular momentum of the atmosphere in each direction:

$$h_1 = -\int R\left[u\sin\phi\cos\lambda - v\sin\lambda\right]dM \quad (8)$$

$$h_2 = -\int R\left[u\sin\phi\sin\lambda + v\cos\lambda\right]dM \quad (9)$$

$$h_3 = \int Ru\cos\phi dM \quad (10)$$

$$(11)$$

Here $R = 6371.0$ km is the radius of the Earth, $\Omega = 7.292115\times10^{-5}$rad/s the average rotation rate, and $g = 9.81\text{m/s}^2$ is the acceleration due to gravity. $C = 8.0365\times10^{37}\text{kgm}^2$ and $A = 8.0101\times10^{37}\text{kgm}^2$ are the axial and next-largest principal moments of inertia of the solid Earth, and $C_m = 7.1236\times10^{37}\text{kgm}^2$ is the principal inertia tensor component of the Earth's mantle [*Gross*, 2009].

The equatorial excitation functions can be easily mapped to equivalent polar motion by a rotation of the reference frame:

$$p_1 + \frac{\dot{p_2}}{\sigma_0} = \chi_1 \tag{12}$$

$$-p_2 + \frac{\dot{p_1}}{\sigma_0} = \chi_2, \tag{13}$$

where σ_0 represents the Chandler frequency, an intrinsic wobble frequency of the solid Earth.

The axial excitation function χ_3 corresponds to unit changes in the rate of rotation of the Earth, and therefore also unit changes in the length of a day (LOD):

$$\frac{\Delta\text{LOD}}{\text{LOD}_0} = \Delta\chi_3, \tag{14}$$

where $\Delta\text{LOD} \equiv \text{UT1} - \text{IAT}$ denotes anomalies in the length-of-day.

Insert description of the transfer functions here.

Note that in the axial AAM terms [(6) and (10)], the zonal integral is uniform, with no weighting function applied. In practice, this means that mass anomalies tend to cancel one another out in the zonal integral, with the result that the axial mass excitation (6) is usually several orders of magnitude smaller than the axial wind excitation (10) (CITE).

Nearly the opposite is due for the equatorial terms [(4)-(5) and (8)-(9)]. Here, longitudinal asymmetry determines the magnitude of the excitation. The mass excitation typically outweights the wind excitation by a few factors for the equatorial terms.

It can be seen that, because of the way they are defined, the three ERPs represent almost unique aspects of the atmospheric dynamics. ΔLOD mostly reflects changes in zonal winds in the tropics and subtropics. Thus it is not surprising that signals corresponding to the

MJO (CITE), the QBO (CITE), and ENSO (CITE) can be seen in the timeseries of observed ΔLOD.

Of the polar motion angles, p_1 largely reflects surface pressure variations over the oceans, and p_2 over the continents. The effect of short-timescale surface pressure variations over the ocean tend to be evened out by corresponding displacement of the ocean surface (the so-called "inverse barometer" effect), reducing the total angular momentum transfered to the Earth. Sub-annual p_1 variations therefore depend largely on other sources of AM. — this statement makes no sense. Look at Henryk's paper and sort out what really happens with p_1. In contrast, p_2, which is strongly weighted over land, has a pronounced annual cycle due to the yearly appearance of the Siberian High (CITE) and tends to show strong negative anomalies in the two months preceding sudden stratospheric warmings [*Neef and Matthes*].

2.2.2. Radiosonde Observations

An analysis of the impact of ERP observations is not very useful unless the results are compared to impact of more standard meteorological observations. It is interesting to ask whether the ERPs deliver any information about the true state that is not already given by the multitude of observations that regularly observe the atmosphere, both from space and from the ground.

As a rough estimate of the existing, meteorological observing system, we have generated a grid of hypothetical radiosonde observations across the Earth at regular intervals. The horizontal grid is shown in Fig. 1. Comment on RS vertical distribution, and also why the grid looks the way it does.

Of course, in reality the global distribution of radiosonde observations is nowhere near as dense as in Fig. 1, especially over the oceans. However, the observing network in Fig. 1 gives us a good rough approximation of the existing meteorological observing system, which is quite dense. Check this and cite it.

2.3. Perfect-model experiments

In this study we perform so-called perfect-model experiments, wherein the "truth" is actually a realization of the model, and observations are generated from this realization with known error statistics. Experiments are performed with an 80-member ensemble, which itself is generated from one full year of assimilation of the uniform grid of radiosonde observations described in Section 2.2.2.

For our experiments, observations of χ_1, χ_2, and χ_3 are generated every 24 hours. This simulates the true observations of the ERPs (p_1, p_2, and ΔLOD), (ΔLOD isn't really the observation .. it's UT1-UTC – but what are they?) which are available once daily (CITE).

It is common in ensemble assimilation to localize the analysis increment, i.e. to limit the impact of an observation in space by setting to zero spatial covariances that are prone to large relative errors *Houtekamer and Mitchell* [1998]. Because the assimilated AAM components are integrals of the global atmospheric state, they are not localized in the horizontal dimensions. However, it was found that assimilation of the AAMs without any localization results in large, spurious analysis increments in the winds at the highest model levels, above 50 hPa or so. The low pressure at these high altitudes means that very large swings in the wind are required to achieve small changes in angular momentum. The

initial spread of the ensemble is also largest above 50 hPa since no radiosonde observations were available at these altitudes in the preconditioning of the ensemble.

In order to prevent spurious analysis increments at upper levels, we therefore apply a boxcar localization function in the vertical, setting all covariances, and thereby all analysis increments, to zero above the 50hPa level.

The main evaluation diagnostic will be root mean square error (RMSE) between the ensemble mean the the true state. To evaluate how much information is actually gained from assimilation in each case, the RMSE for each case will be shown relative to o a case where the 80-member initial ensemble is evolved forward in time without assimilation, hereafter known as the"No-DA" run.

Cite for the principle of localization.

3. Results

3.1. Prior and Posterior fit to Observed ERPs

Figure 2 shows the fit of the ensemble to the observed ERP excitation functions in each of the four main experiments outlined in Section 2.3. The case of no assimilation (Fig. 2(A)) starts out with the ensemble clustered closely around the true ERPs. The ensemble spreads noticeably after about a week, and by the end of January, the ensemble mean lacks any of the short-timescale features of the true ERPs.

When ERPs are assimilated (Fig. 2(B)), the ensemble members naturally agree much more in their predicted ERPs. Thus the assimilation of ERPs is successful in the sense that the wind and surface pressure fields in each ensemble member are nudged enough to give each ensemble member an AAM vector that is close to what is observed. However, the

relative success in fitting the ERPs does not automatically imply that the state variables themselves are closer to the true state. This will be investigated in the following section.

An even greater contrast is seen when radiosonde observations are assimilated (Fig. 2(C)). Here the true ERPs are matched closely for all ensemble members, for the entirety of the assimilation run, even though no ERPs are assimilated. is there any point in showing this case? the fit is so perfect here that we don't really need ERPs.

3.2. Error reduction in wind and pressure fields

A comparison between the NODA and ERPDA experiments in terms of the model state space is given in Figures 3-5. Fig. 3(a) shows the RMSE in zonal wind (see Section 2.3), averaging over all latitudes and longitudes, as a function of height and time, in the NODA experiment. As in the corresponding observation-space plots [Fig. 2(A)] the error begins to spread noticeably after about a week, and saturates after about a month. Error growth is strongest in the tropospheric jets (around 300hPa) and near the model lid.

Fig. 3(b) shows the same but for assimilation of ERPs. Here the error growth is similar but slightly weaker, especially during the first few weeks. The reduction of error between NODA and ERPALL is shown in Fig. 3(c). It can be seen that assimilating ERPs reduces the error most of all at the top of the model, and visible error reduction lasts through about the end of February at which point the assimilation of ERPs actually *increases* the error.

Fig. 3(d) shows the innovation (Prior-Posterior) at each analysis time. The innovation, like the error reduction, is also strongest near the model top. The innovation is generally strongest when the true error is largest, which means that the filter correctly chooses a strong adjustment at times when the error is largest. However, while this results in a large

error reduction early on in the assimilation period, it increases error towards the end of the assimilation period.

[Insert explanation for why increments are concentrated up high.]

Figure 4 examines what happens to the wind at 300hPa as the assimilation progresses. This figure is similar to Fig. 3, but now showing 300hPa wind as a function of latitude and time. Again, the grown of error is slower when ERPs are assimilated [Fig. 4(b)] than with no assimilation [Fig. 4(a)], and we see visible error reduction through January and February [Fig. 4(c)].

Figure 5 is similar to Fig. 4, but showing surface pressure. Here the error growth, and the error reduction brought about my the assimilation of the ERPs, are largely at latitudes about 50°N. Why is that?

3.3. ...anything else...

Acknowledgments. (Text here)

References

Anderson, J., T. Hoar, K. Raeder, H. Lui, N. Collins, R. Torn, and A. Avellano (2009), The data assimilation research testbed: A community facility, *Bull. Am. Met. Soc.*, pp. 1283–1296, doi:10.1175/2009BAMS2816.1.

Anderson, J. L. (2001), An ensemble adjustment filter for data assimilation, *Mon. Wea. Rev.*, *129*, 2884–2903.

Anderson, J. L., and N. Collins (2007), Scalable implementations of ensemble filter algorithms for data assimilation, *J. Atmos. Oceanic Technol.*, *24*, 1452–1463.

Barnes, R., R. Hide, F.R.S., A. White, and C. Wilson (1983), Atmospheric angular momentum fluctuations, length-of-day changes and polar motion, *Proc. Roy. Soc. London*, *387*, 31–73.

Gross, R. S. (2009), Earth rotation variations - long period, in *Geodesy, Treatise on Geophysics*, edited by T. Herring, pp. 239–294, Elsevier.

Houtekamer, P., and H. L. Mitchell (1998), Data Assimilation Using an Ensemble Kalman Filter Technique, *Monthly Weather Review*, *126*(1969), 796–811.

Lehmann, E., and P. Nevir (2012), Uncertainties in relative angular momentum computed from zonal winds in reanalysis data, *J. Geophys. Res.*, *117*, D09,101.

Neale, R. B., C.-c. Chen, P. H. Lauritzen, D. L. Williamson, A. J. Conley, A. K. Smith, M. Mills, and H. Morrison (2011), Description of the NCAR Community Atmosphere Model (CAM 5.0), *National Center for Atmospheric Research Tech. Rep.*, (NCAR/TN-486+STR.), 268.

Neef, L. J., and K. Matthes (), Sudden stratospheric warmings excited Earth rotation variations, *J. Geophys. Res.*, submitted.

Raeder, K., J. L. Anderson, N. Collins, T. J. Hoar, J. E. Kay, P. H. Lauritzen, and R. Pincus (2012), DART/CAM: An ensemble data assimilation system for CESM atmospheric models, *J. Clim.*, doi:10.1175/JCLI-D-11-00395.1, in press.

Saynisch, J., and M. Thomas (2012), Ensemble Kalman-Filtering of Earth rotation observations with a global ocean model, *Journal of Geodynamics*, *62*, 24–29, doi: 10.1016/j.jog.2011.10.003.

Saynisch, J., M. Wenzel, and J. Schröter (2011a), Assimilation of earth rotation parameters into a global ocean model: excitation of polar motion, *Nonlin. Proc. Geophys.*, *18*,

581–585.

Saynisch, J., M. Wenzel, and J. Schröter (2011b), Assimilation of earth rotation parameters into a global ocean model: length of day excitation, *J. Geodesy.*, *85*, 67–73.

References

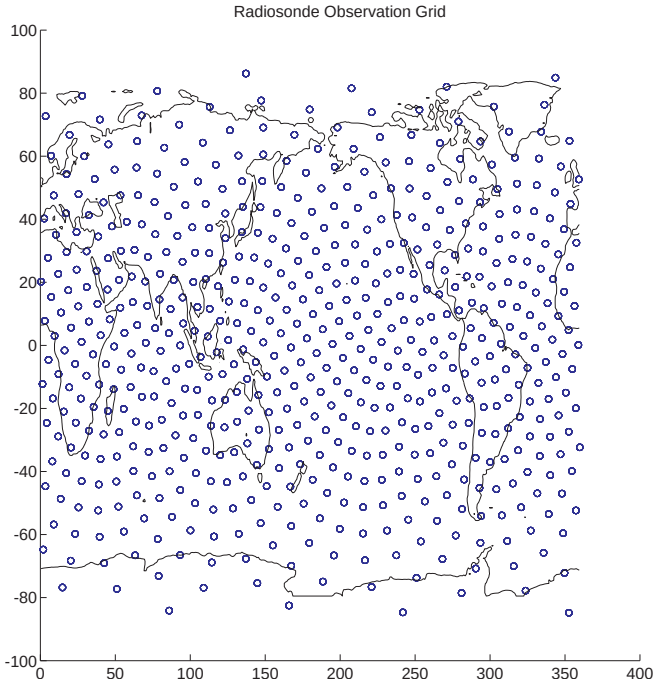

Figure 1. The spatial distribution of hypothetical radiosonde observations.

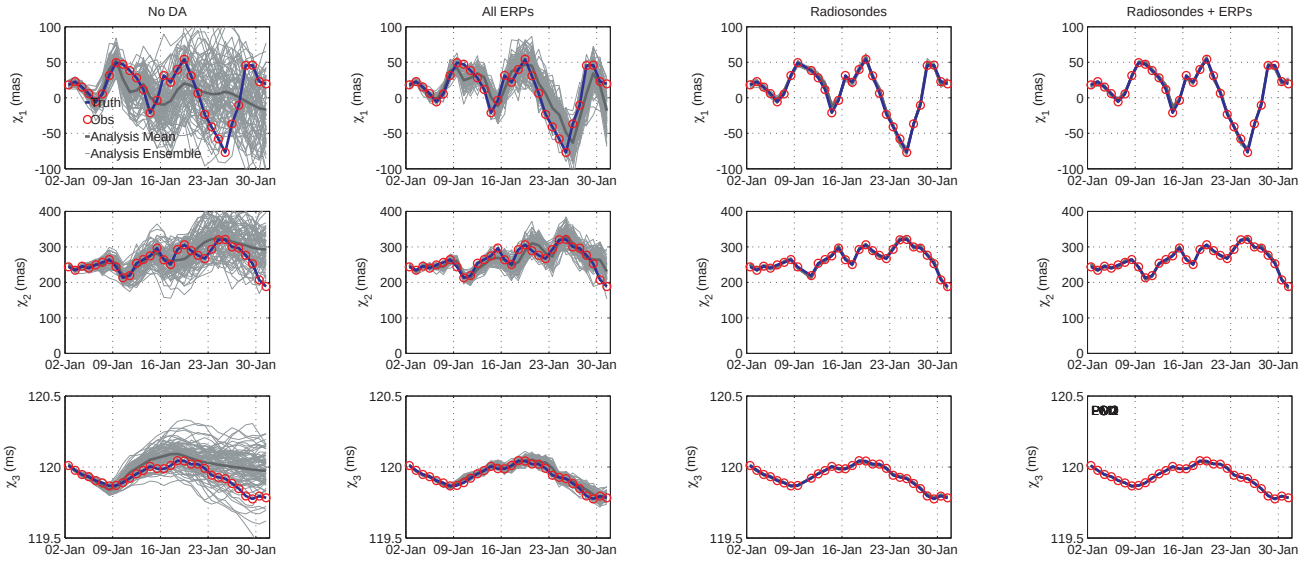

Figure 2. Comparison of the analysis ensemble (gray) and ensemble mean (dark gray) to the true state (blue) and observations (red) of the three ERPs. Each column shows a different experiments: (A) No assimilation, (B) assimilating ERPs only, (C) assimilating radiosonde observations only, and (D) assimilating radiosonde and ERP observations.

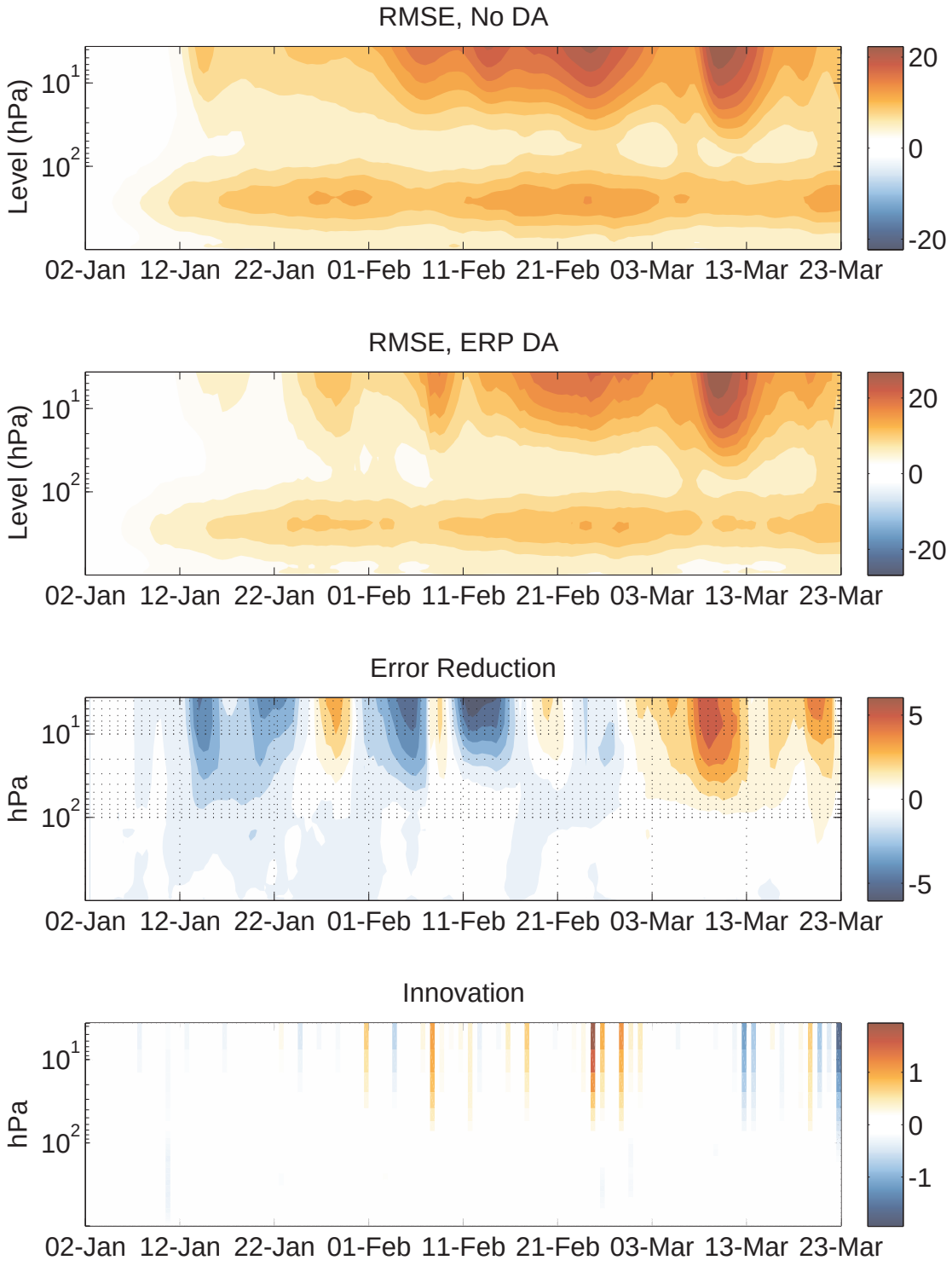

Figure 3. Assimilation diagnostics for the zonal-mean zonal wind, as a function of pressure and time: (a) True error (see text) no assimilation. (b) As above but with 24-hourly assimilation of ERPs. (c) The reduction in error when ERPs are assimilated relative to No-DA. (d) The innovation (posterior-prior).

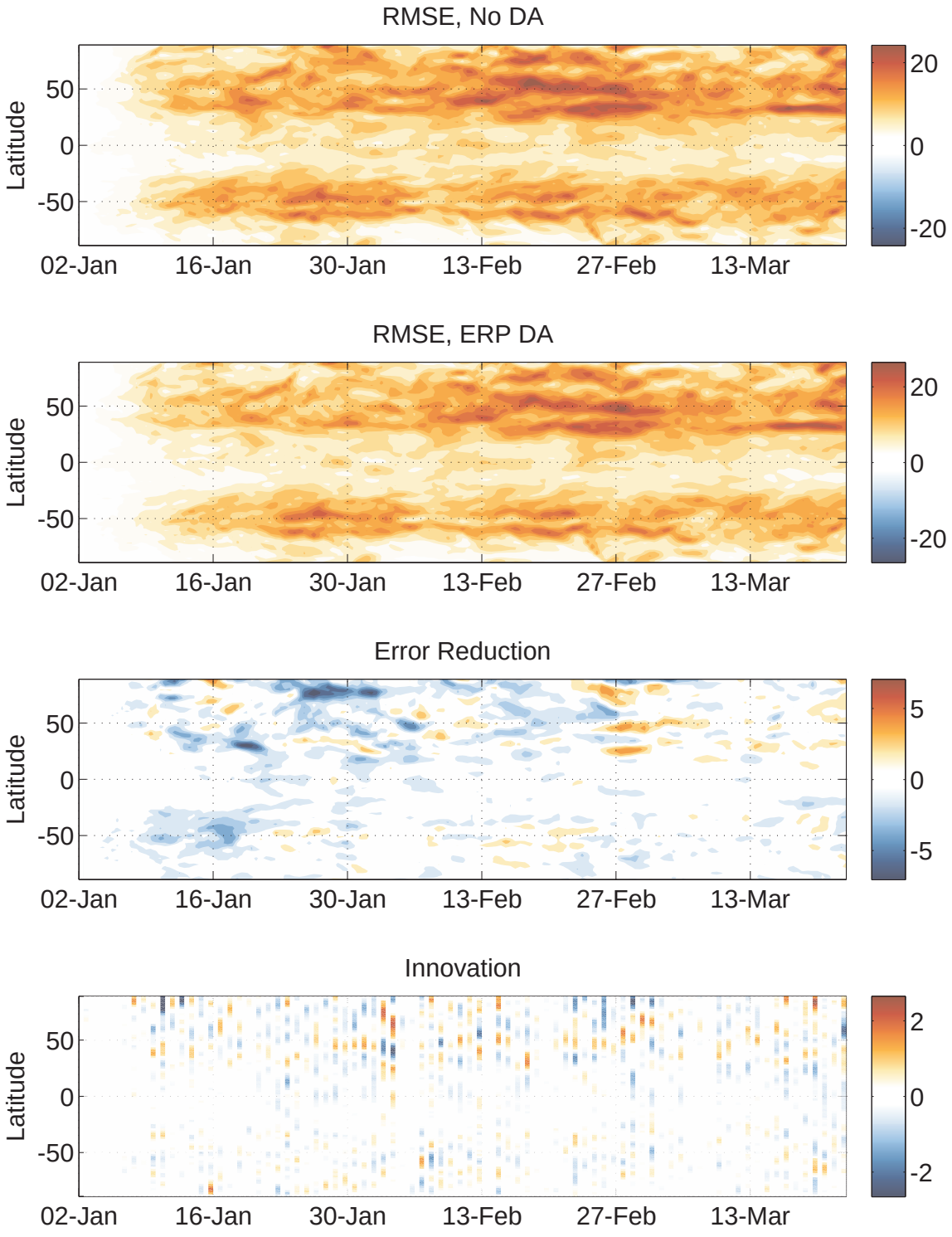

Figure 4. Assimilation diagnostics for the zonal-mean zonal wind at 300hPa, as a function of latitude and time: (a) True error (see text) no assimilation. (b) As above but with 24-hourly assimilation of ERPs. (c) The reduction in error when ERPs are assimilated relative to No-DA. (d) The innovation (posterior-prior).

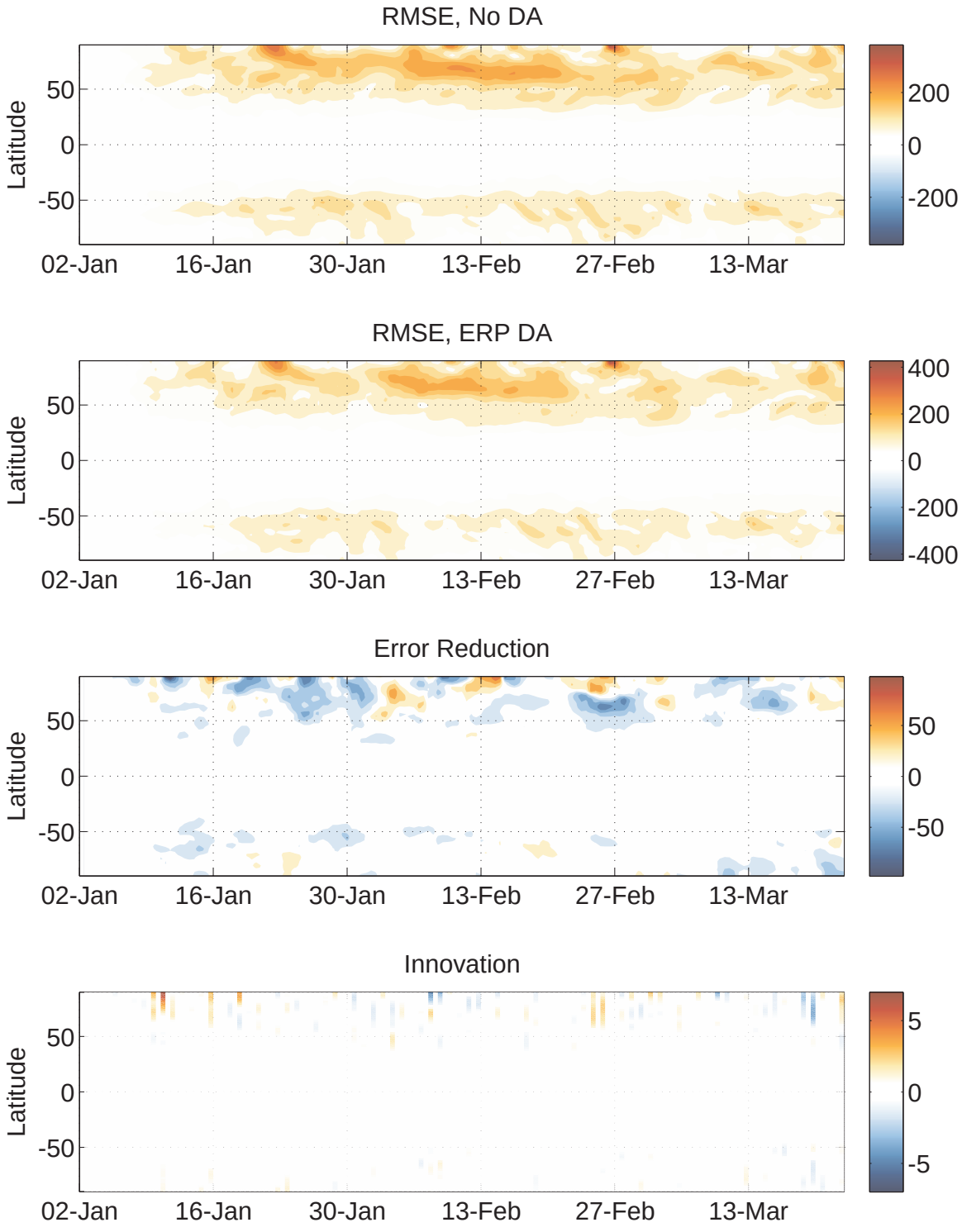

Figure 5. Assimilation diagnostics for the zonal-mean surface pressure as a function of latitude and time: (a) True error (see text) no assimilation. (b) As above but with 24-hourly assimilation of ERPs. (c) The reduction in error when ERPs are assimilated relative to No-DA. (d) The innovation (posterior-prior).

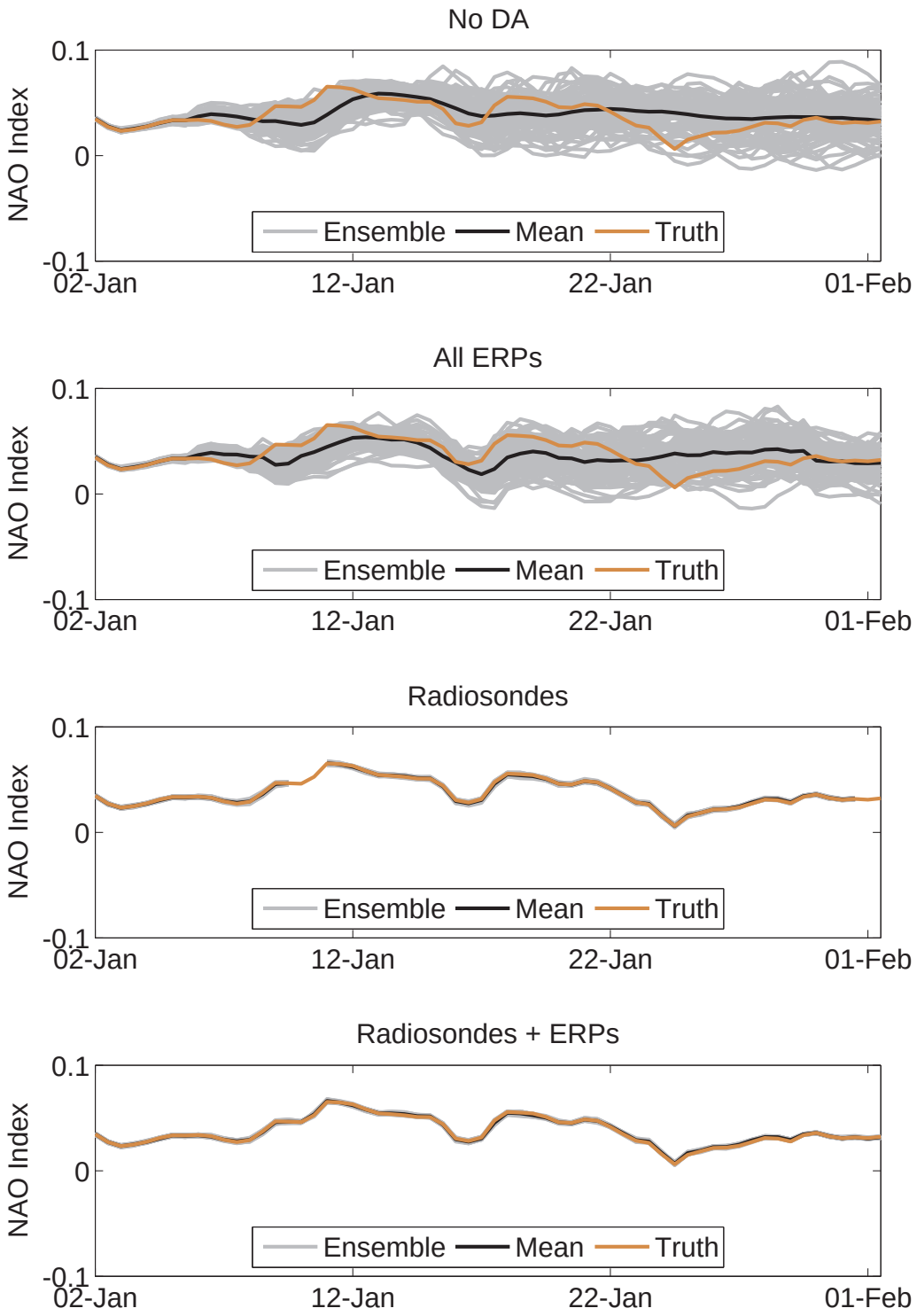

Figure 6. NAO station index (see text) for the posterior ensemble and its mean (gray lines), compared to the true state (blue).